Check for updates

Research Article | Vol. 12, No. 3 / 1 Mar 2022 / Optical Materials Express 1281

Optical Materials EXPRESS

Optical anisotropy of glancing angle deposited thin films on nano-patterned substrates

LINA GRINEVICIUTE,[1,8] TANIA MOEIN,[2,8] MOLONG HAN,[2,8] SOON HOCK NG,[2,9] VIJAYAKUMAR ANAND,[2] TOMAS KATKUS,[2] MEGUYA RYU,[3] JUNKO MORIKAWA,[4,5] MARK J. TOBIN,[6] JITRAPORN VONGSVIVUT,[6] TOMAS TOLENIS,[1,7,10] AND SAULIUS JUODKAZIS[2,5]

[1] *Center for Physical Sciences and Technology, Savanoriu Ave. 231, LT-02300 Vilnius, Lithuania*
[2] *Optical Sciences Centre and ARC Training Centre in Surface Engineering for Advanced Materials (SEAM), School of Science, Swinburne University of Technology, Hawthorn, Victoria 3122, Australia*
[3] *National Metrology Institute of Japan (NMIJ), National Institute of Advanced Industrial Science and Technology (AIST), Tsukuba 305-8563, Japan*
[4] *CREST-JST and Tokyo Institute of Technology, Meguro-ku, Tokyo 152-8550, Japan*
[5] *World Research Hub Initiative (WRHI), School of Materials and Chemical Technology, Tokyo Institute of Technology, 2-12-1, Ookayama, Meguro-ku, Tokyo 152-8550, Japan*
[6] *ANSTO - Australian Synchrotron, Infrared Microspectroscopy (IRM) Beamline, 800 Blackburn Road, Clayton, Victoria 3168, Australia*
[7] *ELI Beamlines, Institute of Physics, The Czech Academy of Sciences, Za Radnicí 835, Dolní Brežany, Czech Republic*
[8] *Contributed equally*
[9] *soonhockng@swin.edu.au*
[10] *tomas.tolenis@ftmc.lt*

Abstract: This study has demonstrated that 3D columnar micro-films/coatings can be deposited over pre-patterned surfaces with sub-micrometer periodic patterns. Four-angle polarisation analysis of thin $(0.4-1\sim\mu$m) Si and SiO_2 films, evaporated via glancing angle deposition (GLAD) at 70° to the normal, was carried out in reflection mode using synchrotron infrared microspectroscopy at the Australian Synchrotron. The angular dependence of absorbance followed $A(\theta)\propto\cos^2\theta$, confirmed for Si substrates patterned by electron beam lithography and plasma etching, which were used to make checkerboard patterns of $\Lambda = 0.4\sim\mu$m period on Si. Retardance control by birefringence of a patterned SiO_2 substrate coated by columnar SiO_2 is promising for UV-visible applications due to the use of the same material to endow polarisation control.

© 2022 Optica Publishing Group under the terms of the Optica Open Access Publishing Agreement

1. Introduction

Deposition at a glancing angle has been known to produce self-shadowing phenomena, which strongly influences the nanostructure of coatings during the growth of low energy films [1,2]. Glancing angle deposition (GLAD) has been investigated in order to control the nanostructural features of the films, such as porosity [3], anisotropy [4,5], and shape [6]. Such coating technology has been used to coat optically anisotropic form birefringent coatings with $\Delta n \equiv n_e - n_o<0$, where the refractive index of the ordinary wave is larger than that of the extraordinary $n_o>n_e$ using amorphous materials. This research has resulted in applications of anisotropic GLAD coatings for the formation of coating-based waveplates [7–9] and zero-angle polarisers [10,11]. In the past few years, more attention has been focused on silica based nanostructures [12–14] due to their large band-gap value and extreme resistance to laser radiation [15,16].

The simplest method to make a birefringent film is to use zig-zag (chevron) folding of growing nanostructures during the GLAD process. By using more sophisticated spatial control of the

#451669 https://doi.org/10.1364/OME.451669
Journal © 2022 Received 22 Dec 2021; revised 18 Feb 2022; accepted 20 Feb 2022; published 1 Mar 2022

Optical Materials EXPRESS

deposition angle along several directions around one axis, it is also possible to deposit films with circular anisotropy. The method shows how optically isotropic materials, such as Si and SiO_2, can be used to make birefringent coatings. Furthermore, GLAD coatings have porosity, which can be controlled by the angle of deposition and this has been shown to increase laser damage thresholds [15]. The average power of ultra-short (sub-1 ps) lasers is increasing by Moore's law over the last 20 years, i.e., doubling every two years $Power \propto Power_{2000} \times 2^{N/2}$, where N is the number of years from the beginning of the trend in 2000 when average power was below ~1 W [17]. Demand for coatings capable of withstanding the high average >1 kW power of ultra-short lasers, required for the most demanding 3D fabrication tasks in terms of throughput and resolution, will continue to increase in the near future. Additionally, as experiments towards laser-driven nuclear fusion becomes more realistic, with a 1.3 MJ yield shot (8 August 2021), being 25 times higher than previous the record [18] registered at the National Ignition Facility (NIF), laser components with extreme optical resistance will be essential to reach even higher energies. Coating prepared using the same material as the substrates are very promising in this respect due to same thermal expansion and simplest adhesion control, and using the same material as the substrate for GLAD coating is currently explored. Also, it has recently been shown that both high electron mobility Ge and high-k dioxides can be used to form metal-oxide-semiconductor (MOS) structures by GLAD [19], which is a promising trend for the miniaturisation of electronics due to reduced leakage current. This is an anticipated development for continuation of the original Moore's law governing development of microelectronics over the last 70 years as the 4-nm resolution node enters industrial use in 2021.

How birefringence of the GLAD coatings is affected by deposition on pre-templated substrates requires better understanding. It could potentially open a pathway towards tailoring birefringence of neighboring regions on the surface down to sub-wavelength ($<\lambda/2$) dimensions with high precision when substrates are prepared by high-resolution techniques, e.g., stepper photo-lithography or electron/ion beam lithography.

Here we reveal optical anisotropy in reflection of 3D columnar films deposited by GLAD. In this study, SiO_2 and Si coatings on Si and glass substrates were examined. Flat and nano-patterned checkerboard substrates were prepared and synchrotron infrared (IR) experiments were carried out on the IR Microspectroscopy (IRM) beamline at the Australian Synchrotron in the mid-IR spectral range.

2. Experimental: samples and procedures

2.1. Samples

Samples for this study were made using electron beam evaporation systems equipped with two stepper motors for GLAD. Two sets of evaporation were performed in order to form anisotropic Si and SiO_2 thin films.

For Si coating, a polycrystalline wafer of Si was broken, melted and used as a source of evaporation. The deposition rate was constantly maintained at 3 Å/s and controlled using a quartz crystal monitoring system. Silicon thin films were coated using a VERA 1100 deposition plant (VTD, Germany).

For SiO_2 thin films, granules of SiO_2 (Merck, Germany) were evaporated at the same 3 Å/s constant rate. Silica thin films were coated using a SIDRABE deposition plant (SIDRABE, Latvia).

In both cases, the thickness of the thin films was 1 μm and the coatings were evaporated using the Serial Bi-Deposition (SBD) technique [4]. During SBD, the substrates were tilted at 70° angle between its normal and the vapour flux. At the same time, half-turn rotations were performed every 6 s in order to enhance the birefringence of the films, as well as to gain a better uniformity of the film thickness. Calcium fluoride (CaF_2) and $\langle 100 \rangle$ orientation p-type Boron doped Si wafers were used as the substrates in both depositions.

Optical Materials EXPRESS

2.2. Polarised synchrotron-IR microspectroscopy

Four-angle polarised IR experiments were performed using synchrotron-IR radiation on the IRM beamline at the Australian Synchrotron (Clayton, Victoria). The IR microspectroscopic system at the IRM beamline consists of a Bruker Vertex 80v spectrometer coupled with a Hyperion 3000 FTIR microscope and a liquid nitrogen-cooled narrow-band mercury cadmium telluride (MCT) detector (Bruker Optik GmbH, Ettlingen, Germany). All the synchrotron-IR spectra were recorded in reflection mode, using a 20× reflecting objective (NA = 0.60) within a spectral range of 3800–700 cm^{-1} and 4 cm^{-1} spectral resolution. Blackman-Harris 3-Term apodization, Mertz phase correction, and a zero-filling factor of 2 were set as default acquisition parameters using the OPUS 8.0 software suite (Bruker Optik GmbH).

Unlike a traditional thermal IR (Globar) source in laboratory-based IR instruments, polarisation of synchrotron-IR radiation has a combination of a linear polarisation along the horizontal slit of the extraction mirror, which is in the plane of the electron beam orbit, and circular polarisation [20]. The two components originate from dipole emission inside the bending magnet and at its edge (at the entrance/exit) [21,22]. The IRM beamline receives a higher proportion of the dipole emission, compared to the edge emission.

Polarisation is defined as x- and y-polarisation in a room frame of reference (a sample plane) and z-axis along the direction of propagation. Data analysis was carried out using OPUS 8.0 software (Bruker Optik GmbH).

3. Results and discussion

The mid-IR and visible spectral response of 3D columnar chevron-type coatings was examined at different polarisations.

3.1. Mid-IR reflectivity of 3D columnar films on flat substrates

First, GLAD zig-zag deposited films of Si and SiO_2 were deposited on flat Si substrates. Thin film coatings measured (or used) in reflection have a doubled optical path for the actual thickness H of the film. This provides high sensitivity for measurements and simpler fabrication. Applications for thinner deposited film on Si substrate can be nano-textured via EBL and other lithography approaches that are already well established.

The orientation dependence of absorbance $A(\theta)$ (all losses measured in reflection) was measured using mesh grid polarisers (made of KRS-5 and ZnSe). They were aligned for high transmittance and rotated synchronously with the sample at a fixed position. The orientation angle θ corresponds to the angle between polariser and sample orientations. This ensured that the mapping data from all the polarisation angles were acquired from the same focal spot of ~ 17 μm in diameter on the sample.

Polarisation analysis of thin columnar zig-zag (chevron) films of SiO_2 deposited by GLAD was carried out in reflection R mode (Fig. 1(a)) in the 3800-700 cm^{-1} spectral window (16.7 - 2.5 μm in wavelength). The absorption bands are plotted in (a) polar and (b) standard 2D spectral maps. Measurements were carried out in the angular range $(0 - \pi)$ and are presented in 2π dependence by repeating measured data (a). This helps to clearly visualise π-folding of the absorbance bands, i.e., $\cos^2\theta$ dependence. Absorption bands typical for SiO_2 are recognisable [23] (reference spectra were measured from a bare Si substrate). Strong absorbance at the Si-O-Si stretching window $\sim 1040 \pm 20$ cm^{-1} was a dominant factor. From the angular dependence of absorbance bands, it is evident that the dependencies are in anti-phase for the vibrational modes at 1027 cm^{-1} and 3268 cm^{-1}.

The same thickness $H \approx 1$ μm columnar coating was made out of Si on Si substrate. Its angular resolved absorbance results are summarised in Fig. 2. The dominant spectral feature is the absorption peak at 2100 cm^{-1}, which had the same $\cos^2\theta$ (π-folding) dependence.

Optical Materials EXPRESS

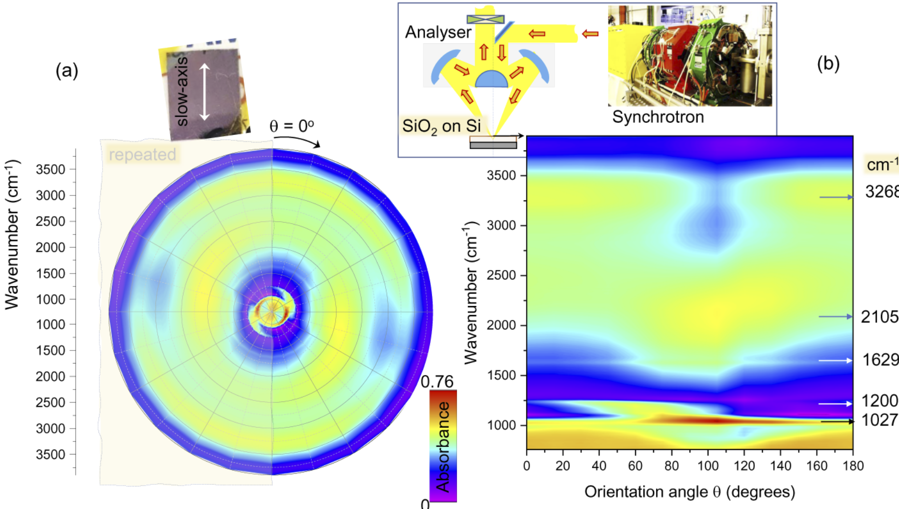

Fig. 1. Maps of angular absorbance $A(\theta)$ of 3D columnar SiO_2-on-Si (see the sample image on the left inset) presented in (a) polar and (b) standard 2D plots. The inset on the top right shows the geometry of the experiment with one analyser screening the reflected beam from the sample. The angular dependence was measured in the range of $0 - \pi$, and was folded to obtain a complete 2π map. The observed absorption bands presented the characteristic of $\cos^2\theta$ dependence. Distinct absorption bands are marked in (b); see details in text.

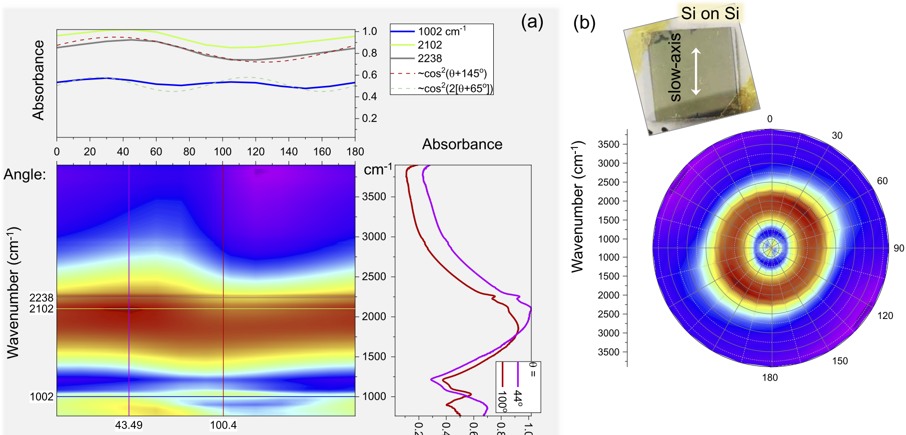

Fig. 2. Maps of angular absorbance $A(\theta)$ of 3D columnar Si-on-Si (see the sample image in the inset of (b)). Data were acquired in reflection mode, and presented in (a) standard and (b) polar plots. The angular dependence was measured in the range of $0 - \pi$ and was folded to obtain a complete 2π map (b). The observed absorption bands presented the characteristic of $\cos^2\theta$ dependence. Distinct absorption bands are indicated in (a); see details in text.

3.2. Mid-IR reflectivity of 3D columnar films on pre-patterned substrates

Since GLAD deposition is typically carried out at large-to-normal angles of $\sim 70°$, the shadowing effect is strong: a step/pillar of height h produces a shadow on the substrate surface $x = h\tan(70°) \approx 2.75h$. Figure 3 shows checkerboard patterns made on Si and SiO_2 by using EBL definition of the etch mask (Cr or PMMA) and subsequent plasma etching. For the PMMA mask,

Optical Materials EXPRESS

it was consumed by the etching process, while for Cr it was removed after etching to the $h \sim 100$ nm depth aimed for this study. In the case of PMMA mask, formation of random nanoscale pattern on Si surface, known as black Si [24,25], was discernible. The imperfect checkerboard patterns were caused by charging and proximity effects during EBL, which can be mitigated and modelled during fabrication [26,27]. The shadowing effect for GLAD nanopatterning of films was the goal of this pattern, so perfect checkerboards were not required.

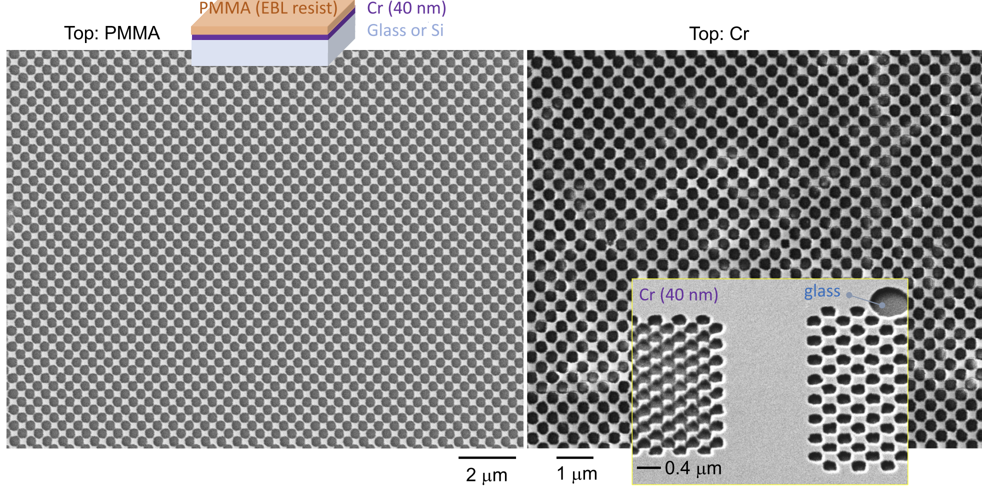

Fig. 3. SEM images of checkerboard patterns made in an EBL resist (PMMA) on a Cr mask layer (left) and after Cr-etch (wet) and dry plasma etch into glass substrate (right). The inset (right) shows a slanted view SEM image of the EBL dose test regions after a glass etching step (Cr mask was not washed out for better SEM imaging). The inset on the top shows the sample structure. Note that a Cr layer was not required for Si patterning via EBL in a PMMA resist, which was used as a sacrificial mask for a $h \sim 100$ nm plasma etch (see Fig. 5).

Figure 4 shows the Si mask and the side-view SEM images of the 3D columnar chevron SiO_2 film deposited at 70° via GLAD. Shadowing of the checkerboard pattern created a distinct pattern of fanning-out SiO_2 columns. The black Si surface with random nano-features was overgrown by SiO_2 and formed the same pattern of columnar film as on the flat Si substrate. However, for the $\Lambda = 400$ nm pattern, the height at which SiO_2 columns merged from neighboring segments was approximately equal to the period. Hence, a strong structural modification of 1 μm-thick film was present.

Absorbance $A(\theta)$ (in reflection) of SiO_2-on-Si (patterned by EBL) is shown in Fig. 5. Similar angular dependence of the very same absorption bands as observed in the 3D columnar films of SiO_2 on the flat Si was observed on the EBL patterned Si substrate (Fig. 5(b)). Since the checkerboard pattern was isotropic, there was no structural anisotropy introduced into the GLAD film. Identical spectral bands, with the same angular dependence typical for absorber $\cos^2\theta$, were confirmed (resemblance to the Malus' law $\cos^2\theta$).

3.3. Optical performance of 3D columnar films on pre-patterned substrates

The performance of a 3D columnar SiO_2 coating was explored in visible wavelengths using angular dependence of transmittance or reflectance at a fixed wavelength to determine retardance and birefringence [28]. The normalised transmittance through a cross-Nicol setup is given by $T(\theta) = \sin^2(2[\theta - \theta_R])\sin^2(\Delta nd/\lambda)$, where θ_R is the orientation of the slow/fast optical axes of a birefringent sample (see the θ-dependence cross section in Fig. 5 for the angular dependence of absorbance in the IR spectral range), θ is the orientation of the polarization of the incident light

Optical Materials EXPRESS

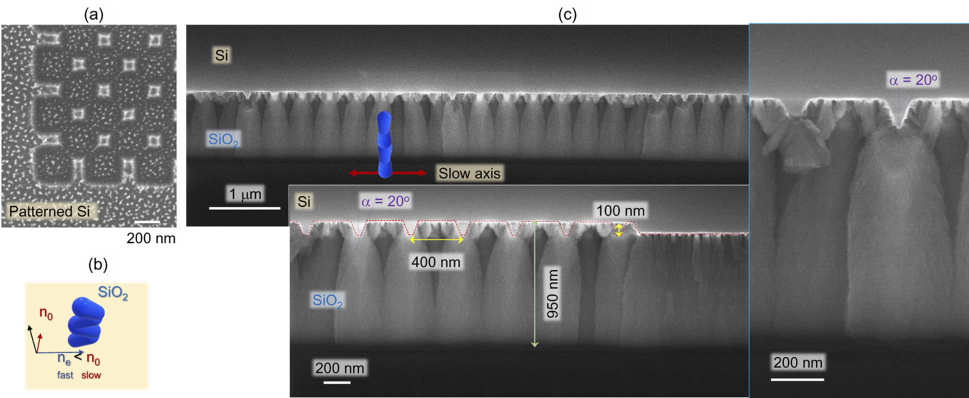

Fig. 4. (a) SEM image of Si substrate after plasma etching using PMMA as a sacrificial mask; EBL was used to define $\Lambda = 4$ μm period checkerboard pattern. (b) Geometry of zig-zag (chevron) coating and conventions of the slow and fast axis. (c) SEM images of side-view cross sections at different magnification (made on a substrate as shown in (a)).

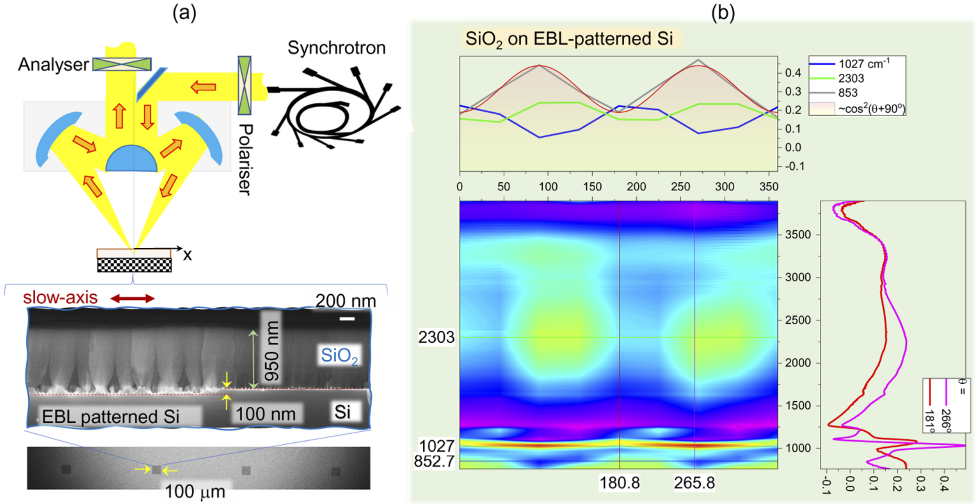

Fig. 5. (a) Polariser-Analyser (P-A) setup used in a reflection mode. Sample's cross-section along the slow axis is shown at the edge of EBL patterned region; top-view SEM image shows 100×100 μm^2 areas. (b) The aligned P-A was used for absorbance A measurements by observing the reflection from checkerboard patterned Si substrate with columnar SiO_2 film. The $\cos^2\theta$ orientation dependence of $A(\theta)$ was observed. Data was measured in $\pi/4$ steps in 2π rotation, while sample was not rotated and a pair of P-A was simultaneously rotated. The EBL templated surface area was 100×100 μm^2 (one write-field) and focal spot size was ~ 17 μm. Reference sample was a flat Si substrate.

and the retardance Δnd is defined by the optical path change through thickness d at birefringence Δn. By measuring $T(\theta)$ or $R(\theta)$ in cross-Nicol arrangement, Δn is determined for the known thickness d.

To introduce structure anistrotropy, a grating-like pattern of $h = 260$ nm depth squares of ~ 350 nm side length was plasma etched into SiO_2-glass and overgrown by $h \approx 400$ nm SiO_2 deposited by GLAD (Fig. 6). Measurement of the optical retardance $\Delta n \times H$ of the thickness H film in transmission was carried out at 400 nm wavelength using the method we developed earlier

Optical Materials EXPRESS

with a light-crystal retarder and 10 nm band pass filters [28]. The method was also verified to quantify birefringence of the black Si formed at an angle to the surface of the Si substrate, which was measured in reflection [29].

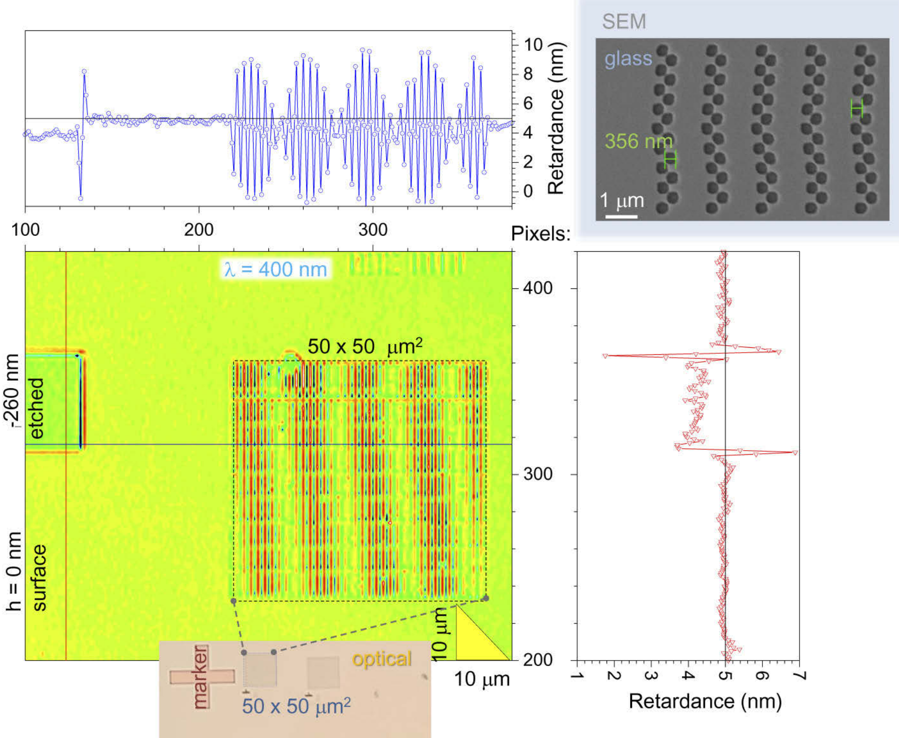

Fig. 6. Optical retardance $\Delta n \times H$ measurement at 400 nm wavelength (in transmission). Retardance in GLAD deposited SiO_2 region 50×50 μm^2 (35 periods of the grating pattern). Resolution of imaging was $0.61\lambda/NA$ = 488 nm at λ = 400 nm and numerical aperture NA = 0.5. A frequency beating pattern (top-panel) is due to under-sampling caused by a finite size of CCD pixels. The baseline was shifted by 5 nm offset in cross sections for clarity. Inset: SEM image of a grating pattern on the glass substrate (Cr mask is removed). The etch depth into glass was h = 260 nm. The optical image (bottom) is after the GLAD deposition of SiO_2 with H = 400 nm thickness; the alignment marker regions are also etched to the same depth as the grating pattern. The birefringence $\Delta n = 3.8 \times 10^{-3}$ (from the cross section shown on the right-side with $\Delta n \times 260$ nm = 1 nm).

With the numerical aperture NA = 0.5 used for the infrared analysis in this study, the objective defines the resolution to be $0.61\lambda/NA$ = 488 nm (Fig. 6) for the light filtered by $\lambda = 400 \pm 5$ nm. The spatial modulation of the patterned structures ~ 350 nm was beyond the resolution limit; however, the grating of Λ = 1.6 μm was optically resolved. The retardance map is shown in Fig. 6. Retardance from the h = 260 nm deep etched region of the marker defined by EBL for reference, was used to determine the birefringence Δn for the measured retardance of 1 nm: $\Delta n = 3.8. \times 10^{-3}$. However, the min-max span of retardance over the grating-patterned region was ~ 7 nm, which translates to $\Delta n = 2.66 \times 10^{-2}$, and is consistent with the birefringence values of columnar SiO_2 films [30]. Since the refractive index is proportional to a mass density $n \propto \rho$, different filling factors of columnar SiO_2 over the plasma etched and pristine surfaces cause modulation of Δn.

Optical Materials EXPRESS

Next, birefringence was measured in reflection from checkerboard patterns of columnar SiO_2-on-glass defined on the cover glass substrate ($\sim$ 150 μm) using EBL. Reflection under white light illumination was used due to the approximately double the retardance caused by a twice-folded optical path. A $\lambda/2$-waveplate at 530 nm wavelength was inserted at $\pi/4$ angle to the polariser and analyser. This cross-polarisation setup visualises retardance by effectively eliminating 530 nm green color out of the light passing through the analyser. Figure 7 shows optical images at different orientation of sample. The inset plot shows an average integrated intensity over the region-of-interest (ROI) for the individual RGB colors. Very small 0.5% changes of retardance was observed in checkerboard regions, which appeared darker. Mean birefringence at the wavelengths $\lambda = 700.0$ nm (red), $\lambda = 546.1$ nm (green), and $\lambda = 435.8$ nm (blue) was calculated from a fit to angular dependence as shown in Fig. 7. From reflectance $R(\theta)$, the retardance was $\Delta nd = 143.30$ nm at the checkerboard region and 142.63 nm from the region on the flat glass substrate. Fit to the angular dependence was made at $\theta = (0 - \pi)$ angle range for $R(\theta)$ over selected ROI (Fig. 7). Considering the thickness of a sculptured SiO_2 film of $d/2 \approx 950$ nm, the difference in birefringence Δn between the patterned and flat regions was negligible. A larger difference in birefringence between checkerboard lines (Fig. 6) up to $\Delta n \approx 2.66 \times 10^{-2}$ was observed as shown above.

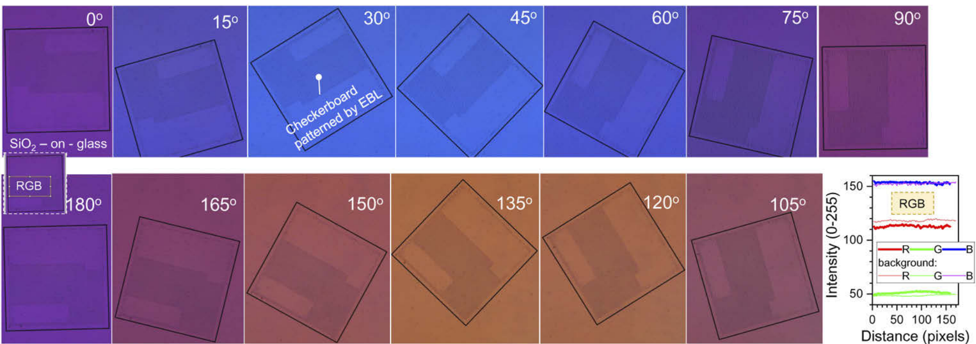

Fig. 7. Optical cross-polarised reflection images of SiO_2-on-glass sample with a $\lambda = 530$ nm waveplate taken with an objective lens ($NA = 0.9$) at different orientation angles θ. The plot of RGB components integrated over a rectangular ROI area on the checkerboard pattern and over a flat region substrate (ImageJ); at $\theta = 0^\circ$. The checkerboard pattern was defined by EBL on cover glass (see Fig. 3). The size of the black square is 50×50 μm^2.

4. Conclusions and outlook

The 3D columnar form birefringent SiO_2 films were characterised at $\lambda = 0.4$ μm, as well as in the mid-IR spectral range (2.5 – 12 μm in wavelength), for their anisotropic properties on flat as well as nano-patterned substrates. It was found that retardance (hence birefringence) of 3D columnar chevron coatings at the short wavelength $\lambda = 400$ nm was modulated by 4 nm for the thick coating $h = 400$ nm. This change of refractive index is related to the mass density changes induced into the 3D columnar film due to the shadowing effect during GLAD deposition. The effect of pattern with period Λ on the morphology of the columnar film was apparent for the same Λ distance into the thickness H of the SiO_2 film.

In addition, Si columnar micro-films on flat Si substrates were characterised in the IR fingerprint region (2.5 – 12 μm) and showed absorption anisotropy following a $\cos^2\theta$ angular dependence. Similar dependence was established for SiO_2 columnar films on patterned Si, and the same dependence was observed for 3D columnar films on flat surfaces [31].

Optical Materials EXPRESS

Funding. Lietuvos Mokslo Taryba (S-MIP-20-61); Core Research for Evolutional Science and Technology (JP-MJCR19I3); Australian Synchrotron (17196); Australian Research Council (DP190103284, LP190100505).

Acknowledgments. This work was supported by the ARC Discovery DP190103284 grant. The project was carried out during the beamtime (Proposal ID. 17196) at the Australian Synchrotron, part of ANSTO. SJ and SHN are grateful for support via ARC Linkage LP190100505 project; JM thanks the JST CREST Grant JPMJCR19I3, Japan. TT and LG are grateful to Research Council of Lithuania (LMTLT) for funding the part of the research, project UnCoatPower (agreement No S-MIP-20-61).

Disclosures. The authors declare no conflicts of interest.

Data availability. Data underlying the results presented in this paper are not publicly available at this time but may be obtained from the authors upon reasonable request.

References

1. H. van Kranenburg and C. Lodder, "Tailoring growth and local composition by oblique-incidence deposition: a review and new experimental data," Mater. Sci. Eng., R **11**(7), 295–354 (1994).
2. M. T. Taschuk, M. M. Hawkeye, and M. J. Brett, *Glancing Angle Deposition in Handbook of Deposition Technologies for Films and Coatings (Third Edition); Science, Applications and Technology* (William Andrew, Applied Science Publishers, 2010).
3. J.-Q. Xi, M. F. Schubert, J. K. Kim, E. F. Schubert, M. Chen, S.-Y. Lin, W. Liu, and J. A. Smart, "Optical thin-film materials with low refractive index for broadband elimination of fresnel reflection," Nat. Photonics **1**(3), 176–179 (2007).
4. I. Hodgkinson and Q. Hong Wu, "Serial bideposition of anisotropic thin films with enhanced linear birefringence," Appl. Opt. **38**(16), 3621 (1999).
5. G. Beydaghyan, K. Kaminska, T. Brown, and K. Robbie, "Enhanced birefringence in vacuum evaporated silicon thin films," Appl. Opt. **43**(28), 5343–5349 (2004).
6. K. Robbie, M. J. Brett, and A. Lakhtakia, "First thin film realization of a helicoidal bianisotropic medium," J. Vac. Sci. Technol., A **13**(6), 2991–2993 (1995).
7. T. Motohiro and Y. Taga, "Thin film retardation plate by oblique deposition," Appl. Opt. **28**(13), 2466–2482 (1989).
8. S. MacNally, C. Smith, J. Spaulding, J. Foster, and J. B. Oliver, "Glancing-angle-deposited silica films for ultraviolet wave plates," Appl. Opt. **59**(5), A155–A161 (2020).
9. L. Grineviciute, M. Andrulevicius, A. Melninkaitis, R. Buzelis, A. Selskis, A. Lazauskas, and T. Tolenis, "Highly resistant zero-order waveplates based on all-silica multilayer coatings (phys. status solidi a 12/2017)," Phys. Status Solidi A **214**(12), 1770175 (2017).
10. A. Doucet, G. Beydaghyan, P. V. Ashrit, and J.-F. Bisson, "Compact linearly polarized ceramic laser made with anisotropic nanostructured thin films," Appl. Opt. **54**(28), 8326–8331 (2015).
11. L. Grineviciute, L. Ramalis, R. Buzelis, and T. Tolenis, "Highly resistant all-silica polarizing coatings for normal incidence applications," Opt. Lett. **46**(4), 916–919 (2021).
12. A. García-Valenzuela, R. Alvarez, J. P. Espinós, V. Rico, J. Gil-Rostra, A. Palmero, and A. R. González-Elipe, "SiO_x by magnetron sputtered revisited: Tailoring the photonic properties of multilayers," Appl. Surf. Sci. **488**, 791–800 (2019).
13. M. Oliva-Ramirez, A. Barranco, M. Löffler, F. Yubero, and A. R. González-Elipe, "Optofluidic modulation of self-associated nanostructural units forming planar bragg microcavities," ACS Nano **10**(1), 1256–1264 (2016).
14. F. V. Grigoriev, V. B. Sulimov, and A. V. Tikhonravov, "Glancing angle deposition of optical coatings: results of the full-atomistic simulation," J. Phys.: Conf. Ser. **1092**, 012046 (2018).
15. T. Tolenis, L. Grinevičiūtė, R. Buzelis, L. Smalakys, E. Pupka, S. Melnikas, A. Selskis, R. Drazdys, and A. Melninkaitis, "Sculptured anti-reflection coatings for high power lasers," Opt. Mater. Express **7**(4), 1249–1258 (2017).
16. T. Tolenis, L. Grinevičiūtė, L. Smalakys, M. Ščiuka, R. Drazdys, L. Mažulė, R. Buzelis, and A. Melninkaitis, "Next generation highly resistant mirrors featuring all-silica layers," Sci. Rep. **7**(1), 10898 (2017).
17. M. Han, D. Smith, S.-H. Ng, V. Anand, T. Katkus, and S. Juodkazis, "Ultra-short pulse lasers – materials - applications," in *Proceedings of the 2nd International Electronic Conference on Applied Sciences*, 15–31 October 2021, Basel, Switzerland, (MDPI, 2021).
18. K. L. Baker, C. A. Thomas, D. T. Casey, M. Hohenberger, S. Khan, B. K. Spears, O. L. Landen, R. Nora, D. T. Woods, J. L. Milovich, R. L. Berger, D. Strozzi, C. Weber, D. Clark, O. A. Hurricane, D. A. Callahan, A. L. Kritcher, B. Bachmann, L. R. Benedetti, R. Bionta, P. M. Celliers, D. Fittinghoff, C. Goyon, R. Hatarik, N. Izumi, M. Gatu Johnson, G. Kyrala, T. Ma, K. Meaney, M. Millot, S. R. Nagel, P. K. Patel, D. Turnbull, P. L. Volegov, C. Yeamans, and C. Wilde, "Hotspot parameter scaling with velocity and yield for high-adiabat layered implosions at the national ignition facility," Phys. Rev. E **102**(2), 023210 (2020).
19. H. M. Singh, Y.-Y. Lim, and P. Chinnamuthu, "Electrical and dielectric parameters in TiO_2-NW/Ge-NW heterostructure MOS device synthesized by glancing angle deposition technique," Sci. Rep. **11**(1), 19837 (2021).
20. M. Ryu, D. Linklater, W. Hart, A. Balcytis, E. Skliutas, M. Malinauskas, D. Appadoo, Y. Tan, E. P. Ivanova, J. Morikawa, and S. Juodkazis, "3D printed polarizing grids for IR-THz synchrotron radiation," J. Opt. **20**(3), 035101 (2018).

Optical Materials EXPRESS

21. A. W. Chao, K. H. Mess, M. Tigner, and F. Zimmermann, *Handbook of Accelerator Physics and Engineering* (World Scientific, 2013).
22. O. Chubar and N. Smolyakov, "Generation of intensive long-wavelength edge radiation in high-energy electron storage rings," in *Particle Accelerator Conference, 1993., Proceedings of the 1993*, (IEEE, 1993), pp. 1626–1628.
23. S. M. Han and E. S. Aydil, "Detection of combinative infrared absorption bands in thin silicon dioxide films," Appl. Phys. Lett. **70**(24), 3269–3271 (1997).
24. A. Žukauskas, M. Malinauskas, A. Kadys, G. Gervinskas, G. Seniutinas, S. Kandasamy, and S. Juodkazis, "Black silicon: substrate for laser 3D micro/nano-polymerization," Opt. Express **21**(6), 6901–6909 (2013).
25. G. Gervinskas, G. Seniutinas, J. S. Hartley, S. Kandasamy, P. R. Stoddart, and S. Juodkazis, "Surface-enhanced Raman scattering sensing on black silicon," Ann. Phys. **525**(12), 907–914 (2013).
26. G. Gervinskas, G. Seniutinas, and S. Juodkazis, "Control of surface charge for high-fidelity nanostructuring of materials," Laser Photonics Rev. **7**(6), 1049–1053 (2013).
27. L. Ren and B. Chen, "Proximity effect in electron beam lithography," in *Proceedings. 7th International Conference on Solid-State and Integrated Circuits Technology*., vol. 1 (2004, IEEE), pp. 579–582.
28. R. Honda, M. Ryu, J.-L. Li, V. Mizeikis, S. Juodkazis, and J. Morikawa, "Simple multi-wavelength imaging of birefringence:case study of silk," Sci. Rep. **8**(1), 17652 (2018).
29. D. Gailevičius, M. Ryu, R. Honda, S. Lundgaard, T. Suzuki, J. Maksimovic, J. Hu, D. P. Linklater, E. P. Ivanova, T. Katkus, V. Anand, M. Malinauskas, Y. Nishijima, S. Ng, K. Staliūnas, J. Morikawa, and S. Juodkazis, "Tilted black-Si: ~0.45 form-birefringence from sub-wavelength needles," Opt. Express **28**(11), 16012–16026 (2020).
30. L. Grineviciute, H. Badorreck, L. Jensen, D. Ristau, M. Jupé, A. Selskis, and T. Tolenis, "Impact of deposition conditions on nanostructured anisotropic silica thin films in multilayer interference coatings," Appl. Surf. Sci. **562**, 150167 (2021).
31. L. Grineviciute, S.-H. Ng, M. Han, T. Moein, V. Anand, T. Katkus, M. Ryu, J. Morikawa, M. J. Tobin, J. Vongsvivut, T. Tolenis, and S. Juodkazis, "Anisotropy of 3D columnar coatings in mid-infrared spectral range," Nanomaterials **11**(12), 3247 (2021).